Lead and slant on the geometry of coiling in gastropods

Ido Filin *

* Corresponding author. E-mail: ido@filin.fi

Running headline: Geometry of coiling.

Supplementary material: SI appendix.

The author(s) declare(s) no conflict of interest.

This manuscript was compiled on 29 April 2026.

Abstract

Molluscan shells have been studied with various geometric models. Here I show that *lead angle*, the defining slope of a conical helix, emerges as a more useful parameter in morphometric analyses and (adaptationist) interpretation of covariation in coiling parameters. The widely used apical semiangle becomes redundant and uninformative, a passive consequence of taxon-specific lead angles and plasticity in growth (expansion rate). Treating coiled shells as conical helices, and extending to *logarithmic slant helices* (curves of precession), provides insights into ontogenetic allometry, irregular coiling, previously formulated shell models, and unifying fixed- and moving-frame approaches.

Keywords: allometry, conchology, logarithmic spiral, ontogeny, slant helix, theoretical morphology,

Note

The equiangular, or logarithmic, spiral has a long and distinguished history, going back to Descartes, Torricelli, Christopher Wren, Newton, Halley, and the Bernoullis (Thompson [1942] 1992; Archibald 1918; Hammer 2016). Its application in biology, however, only picked up with Canon (Henry) Moseley and Carl Friedrich Naumann around 1840, who applied it to the study of molluscan shells, largely due to the rapid development of paleontology in the 19th century (Moseley 1838, 1842; Naumann 1845; Thompson [1942] 1992; Raup 1966; Vinarski 2014). Much of this earlier work on modeling and measurement of shells is thoroughly and eloquently summarized in D'Arcy Thompson's *magnum opus* "On Growth and Form" (Thompson [1942] 1992).

In "The geometry of coiling in gastropods", Raup (1961) sketched an earlier version of his parameter set for coiled geometries, that would later develop into theoretical morphology and the morphospace concept (Raup & Michelson 1965; Raup 1966, 1967; McGhee 1999; Gerber 2017). Essentially, though, Raup's model is a reformulation of the original *conispiral* parametrization of Moseley (1838) and Thompson ([1942] 1992) — a logarithmic spiral wrapped around a cone of *apical semiangle*, β, rather than winding on a plane (planispiral coiling, $\beta \to \pi/2$; Fig. 1A,D). Its defining feature is a fixed *spiral angle*, α, between the tangent of the spiral and its pole (or apex of the cone; hence, equiangular; Fig. 1A).

Conical logspirals also arise from fixed standardized *curvature* and *torsion* in the *differential geometric* formulation of Okamoto (1988), a local (moving) frame analysis (Fig. 1B) that he named the 'growing tube' model. A third alternative parameterization views the conical logspiral as a *conical helix* (Fig. 1C). The defining feature of a helix (more accurately, general or generalized helix, or curve of constant slope; Nutbourne & Martin 1988; Scofield 1995; Rice 1998; SI) is the constant angle its tangent makes with some fixed direction. This direction determines the coiling axis, and the constant slope will be measured in this study by the downward angle of the coil, or helical thread, termed *lead angle*, λ in Fig. 1D. (Preserving here the distinction between 'pitch' and 'lead', in the case of

multi-thread or -strand helical structures, i.e., double or triple helices, or multi-start screws; see SI for more on terminology). If the coils wrap around a cone ($0 < \beta < \pi/2$), rather than a cylinder ($\beta \to 0$; the familiar circular helices of springs and corkscrews), such a conical helix is also a logarithmic conispiral. I dub this third parameterization *conihelical*.

In the words of D'Arcy Thompson, "It seems a complicated affair; but it is only a pathway winding at a steady slope up a conical hill … a certain ensemble, or bunch, of these spiral curves in space constitutes the self-similar surface of the shell" (Thompson [1942] 1992). In this note, I explore how conical helices and their "steady slope", or lead angle, have underappreciated implications to morphometrics, interpretations of covariation in coiling parameters, and unifying *fixed-* and *moving-frame* approaches to theoretical morphology. In addition, conical helices can be extended to *slant helices*, particularly the *logarithmic slant helix* that I present here, to gain better understanding of ontogenetic allometry, irregular coiling, and previously formulated models of allometric spirals.

As hinted in the above quote, a shell is not a single conispiral, but a three-dimensional structure made of "a bunch" of such spirals — the *multispiral* approach (Fig. 1E; also called multivector; Thompson [1942] 1992; Bayer 1978; McGhee 1978, 1999; Savazzi 1990). Alternatively, a shell can be described by a *generating curve*, a closed figure that sweeps through space along a spiral *centerline* (Fig. 1F; Thompson [1942] 1992; Raup 1961, 1966; Okamoto 1988; roughly corresponding to the 'aperture trajectory' of Stone 1995, 'curve-skeleton' of Monnet *et al.* 2009, 'ontogeny axis' of Liew & Schilthuizen 2016, or 'internal spiral' of Larsson *et al.* 2020). While called fictitious and an artificial construction (Moulton *et al.* 2012; Moulton & Goriely 2012), the centerline seems a necessary evil, being a central feature of most theoretical morphological and morphometric shell models (Raup 1966; Okamoto 1988; Liew & Schilthuizen 2016; Larsson *et al.* 2020; eventually, also Moulton & Goriely 2012 use it).

In self-similar isometrically growing conihelical shells, the different spirals that make the shell's surface, by geometric necessity, differ in spiral angle, α, apical semiangle, β, and lead angle, λ (Fig. 1E). However, they all share a single common value of exponential *expansion*

rate, γ, with respect to revolution angle, θ (Illert 1983). Given linear measures of shell size, such as aperture size, a and b (Fig. 1F), centerline radius and height, r and z (Fig. 1D), or centerline *arclength*, s, measured from the pole (or conical apex), one can define separate expansion parameters for each. However, for self-similar conihelical shells, these expansion rates are all equal, $\gamma_s = \gamma_a = \gamma_b = \gamma_z = \gamma_r = \gamma$. Alternatively, growth and size can be measured w.r.t arclength, s, rather than revolution angle, θ. For example, the relations $a(s)$ and $b(s)$, for aperture size, introduce Ackerly's (1989*a*) *dilation* parameter, which I denote here by $q_a = \mathrm{d}a/\mathrm{d}s$ and $q_b = \mathrm{d}b/\mathrm{d}s$. In isometric conihelical shells, q_a and q_b are constants, representing the opening angles of the expanding 'trumpet' or 'cone' (Ekaratne & Crisp 1983; Ackerly 1989*a*; Vermeij 2002) that is coiled upon itself to make the spiral shell. Dilation factors for centerline r and z are just $q_r = \cos\alpha \sin\beta$ and $q_z = \sin\lambda = \cos\alpha\cos\beta$.

A set of formulas relates the conispiral, conihelical, and differential geometric parameterizations to each other and to expansion rates. One such formula is the aforementioned expression for q_z, relating lead angle, λ, to spiral angle, α. For expansion rate,

$$\cot\alpha \sin\beta = \gamma \qquad [1]$$

(Moseley 1842; Thompson [1942] 1992; Raup & Graus 1972; Løvtrup & von Sydow 1974; Ekaratne & Crisp 1983; Illert 1983). Gastropod shells usually exhibit several complete whorls. Consequently, expansion rate is typically small, $\gamma \leq 0.2$ (Thompson [1942] 1992; Cameron 1981), leading to a similar, approximate, expression for the conihelical parameterization,

$$\tan\lambda \tan\beta \approx \gamma \qquad [2]$$

(the exact expression being $\tan\lambda\tan\beta = \gamma/\sqrt{1+\gamma^2}$; see SI for discussion of approximation errors), demonstrating the three-way covariation of expansion rate, apical semiangle and lead angle.

Many empirical studies of shell coiling, in the past 50 years, have provided estimates of Raup's T and W parameters; or in terms of this study, $\tan\beta = 1/T$ and $\gamma = \ln W/2\pi$ respectively. Covariation of $\tan\beta$ and γ may point to adaptation, such as for mechanical

strength, postural stability or economical shell construction (Raup 1966; Noshita *et al.* 2012; Okabe & Yoshimura 2017; Páll-Gergely *et al.* 2024), and is usually interpreted through Raup's (1966) condition for tight coiling, or whorl overlap, $\tan\beta > \sinh(\pi\gamma)$, given circular apertures (SI). (Alternatively, $\sin\beta > \tanh(\pi\gamma)$; corresponding to the expression by Clarke *et al.* 1999, accounting for the typo in their equation, and the difference in definition of apical angle; SI). However, for small γ, typical of most gastropods, the whorl overlap boundary is practically indistinguishable from the seemingly arbitrary condition $\lambda < \arctan(1/\pi)$ (0.318 or 17.66°; Fig. 2A; SI). Similar conditions can be formulated for non-circular apertures (SI). A geometric constraint on lead (or spiral) angle, combined with variation in growth rate (shell expansion), can therefore produce, given Eq.[2], the empirically observed direct relation between $\tan\beta$ and γ.

Past hints to the relative constancy of lead angles can also be glimpsed from observations of ontogenetic patterns, where measurements of $\tan\beta$ and γ at different whorls, or developmental stages, vary together so to preserve an almost fixed ratio (e.g., Newkirk & Doyle 1975; Hutchinson 1989; Clarke *et al.* 1999). In particular, Ekaratne & Crisp's (1983) shell-height-to-arclength-ratio contains a $1/\sec\alpha\sec\beta$ factor, which is just $q_z = \sin\lambda$ of this study. In fact, their formula can be rewritten as $H/s = z/s + b/s = q_z + q_b = \sin\lambda + q_b$ (SI). Lead angle, therefore, a defining feature of conical helices, emerges as a more useful parameter for interpreting morphometric (co)variation (Fig. 2B). Variation in apical semiangle (β; Fig. 2A) follows as a passive consequence of growth (variation in γ) and geometry (lead angle, λ) of the expanding centerline spiral (Eq.[2]).

Lead angle, however, is expected to vary ontogenetically to some degree. For example, Savazzi (1990) discussed deviated protoconchs (see also Frýda & Ferrová 2011); van Osselaer & Grosjean (2000) fitted conispirals piecewise to several species, and showed three ontogenetic phases — protoconch, and early and late conispiral phases — with different coiling parameters; and Newkirk & Doyle (1975) reported values of coiling parameters for embryos and adults in a study of geographic variation in the rough periwinkle, *Littorina saxatilis* (Fig. 2).

Variation in lead angle can be further understood by considering the differential geometric parameterization. In helices, coiling angle per unit of centerline arclength, $\mathrm{d}\theta/\mathrm{d}s$, is measured by the norm of the *Darboux vector*, $\mathbf{u} = u\hat{\mathbf{u}}$, the rotation vector of the Frenet frame along its defining space curve (Fig. 1B; Chouaieb *et al.* 2006; Goriely 2017). In generalized helices, $\hat{\mathbf{u}}$ coincides with the fixed coiling axis. The norm of the Darboux vector, $\|\mathbf{u}\| = u$, is the 'compound curvature' of Nutbourne & Martin (1988), the 'first alternative curvature' of Güzelkardeşler & Şahiner (2024), and the familiar $\sqrt{\kappa^2 + \tau^2}$ of differential geometric literature (also D_G and A_G of Noshita 2014 and Noshita *et al.* 2016, who used Okamoto's growing tube formulation; clearly related in their experssions to angular rate, $\mathrm{d}\theta/\mathrm{d}s$). In this note, I refer to u as *local coiling*. The constant lead angle of general helices is determined by the torsion-curvature ratio, $\tan\lambda = \tau/\kappa$, $\kappa = u\cos\lambda$, and $\tau = u\sin\lambda$.

Conical helices are further defined by local coiling that is inversely proportional to arclength, s (Nutbourne & Martin 1988). We can, therefore, write $u = \tilde{u}/s$, where $\tilde{u}$ is constant dimensionless *standardized local coiling* (though the 'standardization' here is different than Okamoto's). Arclength expansion rate, γ_s, is then related to (standardized) local coiling by the simple and intuitive relation $\gamma_s = 1/\tilde{u}$ (SI). As local coiling and curvature increase, the conical helix coils tighter, and less arclength growth and radial expansion is gained per full revolution. Hence, more whorls are required for a specified amount of (relative) growth. This helps to explain the association of high-spired species with large numbers of whorls (Cain 1980) and Gould's so-called "jigsaw constraint", originally observed in his study of *Cerion* (Gould 1989; Béguinot 2021).

Allometric modifications of conical helices, such as the logarithmic *helicospiral* model, derived many times in various guises (essentially, $\gamma_z \neq \gamma_r$; Kohn & Riggs 1975; Bayer 1978; Cortie 1989; Schindel 1990; Savazzi 1990; Fowler *et al.* 1992; Stone 1995; Tursch 1997; van Osselaer & Grosjean 2000; Urdy *et al.* 2010; Swan 2015; Larsson *et al.* 2020), and Harary & Tal's (2011)'s 'natural 3D spiral', do not have constant lead angles, and therefore, are not generalized helices. Rate of change in lead angle, $\lambda' = \mathrm{d}\lambda/\mathrm{d}s$, is equivalent to the 'second alternative curvature' of Uzunoğlu *et al.* (2016) and Güzelkardeşler & Şahiner (2024) (see SI).

If $\lambda' \neq 0$, the Darboux vector of local coiling and the fixed coiling axis of the helicospiral do not coincide, as the former now precesses around the latter (Fig. 1G). The precession axis is

$$\begin{aligned} \mathbf{w} &= w\hat{\mathbf{w}} = \mathbf{u} + \lambda'\hat{\mathbf{n}} = u\hat{\mathbf{u}} + \lambda'\hat{\mathbf{n}}, \\ w &= \|\mathbf{w}\| = \sqrt{u^2 + (\lambda')^2} = \sqrt{\kappa^2 + \tau^2 + (\lambda')^2}, \end{aligned} \qquad [3]$$

dubbed here respectively vector and rate of *global coiling*. This total coiling rate contains both a local coiling component, u, and a λ' component (first and second 'alternative curvatures' of Uzunoğlu *et al.* 2016 and Güzelkardeşler & Şahiner 2024; generalized helices are obtained when $\lambda' = 0$).

Four decades ago, Løvtrup & Løvtrup (1988) attempted to "move the β parameter down to the mantle edge". In other words, derive a parameter of global shell shape from local processes occurring at the aperture. Løvtrup & Løvtrup's partial solution was to replace β with the ratio of maximum and minimum growth rates around the aperture. An explanation that Hutchinson (1990) debunked shortly after. Through Eqs.[1] and [2], however, the apical semiangle can indeed be "eliminated", or "moved down" to the aperture, as γ, α, and λ are defined at the growing tip (i.e., tangent) of conispirals, or conical helices. The distinction between fixed- (conispiral and conihelical) and moving-frame (differential geometric) parameterizations, thus, begins to blur.

Another defining feature of fixed-frame models is, for obvious reasons, the fixed coiling axis. Rate of change in the direction of local coiling, $\hat{\mathbf{u}}$, is given by $\hat{\mathbf{u}}' = \mathbf{w} \times \hat{\mathbf{u}} = u\hat{\mathbf{u}} \times \hat{\mathbf{u}} + \lambda'\hat{\mathbf{n}} \times \hat{\mathbf{u}} = \lambda'\hat{\mathbf{n}} \times \hat{\mathbf{u}}$. In conihelical shells $\lambda' = 0$, and the Darboux vector, $\mathbf{u}$, defines the fixed coiling axis. Thus, given starting coiling direction (initial condition), conispiral coiling can be defined by apical and spiral angles, by lead angle and expansion rate, by lead angle and standardized local coiling, $\tilde{u}$, or by Okamoto's standardized curvature and torsion (SI). In all four cases, if parameter values remain fixed, the initial coiling direction is maintained ($\hat{\mathbf{u}}' = 0$), becoming a fixed axis, and self-similar conispiral shells result. That is another metric by which the distinction between fixed- and moving-frame parametrizations seems superfluous.

Irregular coiling, allometry, or other deviations from self-similar conihelical geometry,

always require a change in parameter values (notably, lead angle). Gradual rotation of the local coiling axis, $\hat{\mathbf{u}}$, thus, occurs simultaneously with (transient) change in lead angle ($\lambda' \neq 0$), and by precessing around the vector of global coiling, $\mathbf{w}$ (Fig. 1G). That is, in fact, another direct consequence of conihelical geometry; this time, prescribing a testable hypothesis on how shell geometry can deviate from isometric conihelical. Some evidence in support of this hypothesis appears in Ackerly's (1989*b*) visual and stereographical analyses of *Vermicularia*, which possesses a tightly coiled conispiral juvenile phase, followed by an open-coiled geometry that differs in both coiling axis and lead angle. Similarly, his analysis of *Distorsio* shows that lead angle varies among consecutive episodic growth increments, while the coiling axis precesses with an angular radius of roughly four to seven degrees. Savazzi (1996) provides examples from several species of *Tenagodus* (syn. *Siliquaria*) and *Vermicularia* that follow the same rule of simultaneous change in coiling axis and in lead angle. Particularly extreme cases occur in microsnails (Clements *et al.* 2008; Liew *et al.* 2014) and in irregularly coiled (heteromorph) ammonoids (Okamoto 1988, 1996).

Initially, the allometric logarithmic helicospiral ($\gamma_z \neq \gamma_r$) seems to contradict the hypothesis, as lead angle increases ($\gamma_z > \gamma_r$) or decreases ($\gamma_z < \gamma_r$), while the coiling axis remains fixed. Similarly, in Harary & Tal's (2011)'s 'natural 3D spiral', lead angle varies smoothly between a starting value, λ_0, and an asymptotic value, λ_∞, at large arclengths; essentially, converging to a conispiral (though adult size and shape may be obtained well before that asymptote is reached). However, when the direction of $\mathbf{w} = u\hat{\mathbf{u}} + \lambda'\hat{\mathbf{n}}$ does not change, it acts as the new fixed coiling axis of the shell; its magnitude, $w = \sqrt{u^2 + (\lambda')^2}$, is the coiling rate around that axis (i.e., revolution angle per unit growth of centerline arclength, $\mathrm{d}\theta/\mathrm{d}s = w = \|\mathbf{w}\|$). This precession of the local moving Frenet frame around a potentially fixed axis, $\hat{\mathbf{w}}$, is another reason why fixed- and moving-frame models should be considered in tandem, as complementary points of view.

The condition of fixed $\hat{\mathbf{w}}$ is satisfied, for example, when local coiling and change in lead angle are both constant, $u = \text{const}$, $\lambda' = \text{const}$. These are the 'modulated curves' of Nutbourne & Martin (1988), better known as 'curves of constant precession' (Scofield 1995). Another

class of curves, in which $\hat{\mathbf{w}}$ is fixed, are the already familiar conical and generalized helices. This is just the degenerate case of $\mathbf{w} = \mathbf{u}$ and $\lambda' = 0$, where the precession vanishes. Extrapolating from both curves of constant precession and curves of constant slope (generalized helices), one obtains a class of curves called *slant helices* that includes the former two as special cases. A necessary and sufficient condition for a slant helix, in the notation of this study, is $\lambda' \propto u$, or $\lambda' = \sigma u$ where $\sigma = \text{const}$ (Izumiya & Takeuchi 2004 ; SI).

We can proceed still one step further, and define the *logarithmic slant helix*, $u, \lambda' \propto 1/s$, or $u = \tilde{u}/s$ and $\lambda' = \sigma\tilde{u}/s$, where σ and $\tilde{u}$ are constants (SI). While the logarithmic slant helix describes an allometrically growing shell, it does share some properties with the isometric conical helix. For example, revolution angle and arclength are similarly related through $\theta \propto \ln(s/s_0)$, and therefore arclength expands exponentially, $s = s_0 e^{\gamma_s \theta}$, where $\gamma_s = 1/\tilde{w}$, $\tilde{w} = \tilde{u}\sqrt{1+\sigma^2}$. Another feature of logarithmic slant helices is that lead angle grows linearly with θ. Consecutive whorls, separated by a full revolution around the coiling axis ($\acute{}\theta = 2\pi$), are always tilted relative to each other by the same amount, $\acute{}\lambda = 2\pi\lambda'/w = 2\pi\sigma/\sqrt{1+\sigma^2}$ (Fig. 1H).

The logarithmic slant helix, thus, is a natural allometric extension of the isometric conical helix, in the sense that, instead of being fixed on the same initial value (λ_0) throughout ontogeny, lead angle grows linearly (i.e., $\lambda(\theta) = \lambda_0 + c\theta$; $c = \text{const}$). In that respect, it is the simplest case of centerline allometry, and provides insight into the more complex variation in other models (helicospirals, $\gamma_z \neq \gamma_r$, or Harary & Tal 2011). Clearly, lead angle cannot grow indefinitely, unless coiling becomes open and irregular. But, in any case, real shells have a finite number of whorls, and therefore, the logarithmic slant helix, like its older cousin, the conical helix, is a useful approximation. In particular, given expressions for centerline height and radius, $z(\theta)$ and $r(\theta)$ (SI), one can simulate such shells graphically (Fig. 1H,I).

Supplementary information

Additonal derivations, explanations, methods, and discussion are are in the supplementary information document.

DATA AND SOFTWARE AVAILABILITY. All data and code are available at https://doi.org/10.5281/zenodo.19763621, for the data analyses (Fig. 2), and at https://doi.org/10.5281/zenodo.19895626, for the `WebGL` application of theoretical morphology of coiled shells (Fig. 1).

References

Ackerly SC (1989*a*). Kinematics of accretionary shell growth, with examples from brachiopods and molluscs. *Paleobiology* 15: 147–164. 10.1017/s0094837300009337.

Ackerly SC (1989*b*). Shell coiling in gastropods; analysis by stereographic projection. *PALAIOS* 4: 374–378. 10.2307/3514561.

Araki A, Noshita K (2023). Theoretical morphological analysis of differential morphospace occupation patterns for terrestrial and aquatic gastropods. *Evolution* 77: 1864–1873. https://doi.org/10.1093/evolut/qpad110.

Archibald RC (1918). The logarithmic spiral (undergraduate mathematics clubs, topics for club programs). *American Mathematical Monthly* 25: 189–193.

Bayer U (1978). Morphogenetic programs, instabilities, and evolution — a theoretical study. *Neues Jahrb Geol Paläont Abh* 156: 226–261.

Béguinot J (2021). Adult shell-size regulation in conispirally-coiled shells: evidence for a widespread negative covariance between whorls growth-rate and the final number of whorls in land snails. *Annual Research & Review in Biology* 36: 95–106. https://doi.org/10.9734/arrb/2021/v36i1030439.

Cain AJ (1980). Whorl number, shape, and size of shell in some pulmonate faunas. *J Conchol* 30: 209–221.

Cameron RAD (1981). Functional aspects of shell geometry in some british land snails. *Biol J*

Linn Soc 16: 157–167. https://doi.org/10.1111/j.1095-8312.1981.tb01648.x.

Chouaieb N, Goriely A, Maddocks JH (2006). Helices. *Proc Natl Acad Sci USA* 103: 9398–9403. https://doi.org/10.1073/pnas.0508370103.

Clarke RK, Grahame J, Mill PJ (1999). Variation and constraint in the shells of two sibling species of intertidal rough periwinkles (gastropoda: Littorina spp.). *J Zool* 247: 145–154. 10.1111/j.1469-7998.1999.tb00978.x.

Clements R, Liew TS, Vermeulen JJ, Schilthuizen M (2008). Further twists in gastropod shell evolution. *Biology Letters* 4: 179 – 182. https://doi.org/10.1098/rsbl.2007.0602.

Cortie M (1989). Models for mollusc shell shape. *South African Journal of Science* 85: 454–460.

Ekaratne SUK, Crisp DJ (1983). A geometric analysis of growth in gastropod shells, with particular reference to turbinate forms. *Journal of Marine Biology Association UK* 63: 777–797.

Fowler DR, Meinhardt H, Prusinkiewicz P (1992). Modeling seashells. *Proceedings of the 19th annual conference on Computer graphics and interactive techniques*, pp. 379–387. 10.1145/133994.134096.

Frýda J, Ferrová L (2011). The oldest evidence of non-coaxial shell heterostrophy in the class Gastropoda. *Bull Geosci* 86: 765–776. 10.3140/bull.geosci.1302.

Gerber S (2017). The geometry of morphospaces: lessons from the classic Raup shell coiling model. *Biol Rev* 92: 1142–1155. https://doi.org/10.1111/brv.12276.

Goriely A (2017). *The Mathematics and Mechanics of Biological Growth*. Springer. https://doi.org/10.1007/978-0-387-87710-5.

Gould SJ (1989). A developmental constraint in *Cerion*, with comments on the definition and interpretation of constraint in evolution. *Evolution* 43: 516–539.

Güzelkardeşler G, Şahiner B (2024). An alternative approach to find the position vector of a general helix. *Celal Bayar University Journal of Science* 20: 54–60. 10.18466/cbayarfbe.1479066.

Hammer Ø (2016). *Perfect Shape: Spiral Stories*. Springer.

Harary G, Tal A (2011). The natural 3d spiral. *Computer Graphics Forum* 30: 237–246. https://doi.org/10.1111/j.1467-8659.2011.01855.x.

Hutchinson JMC (1989). Control of gastropod shell shape: the role of the preceding whorl. *J Theor Biol* 140: 431–444.

Hutchinson JMC (1990). Control of gastropod shell form via aperture growth rates. *J Morphol* 206: 259–264.

Illert C (1983). The mathematics of gnomonic seashells. *Math Biosci* 63: 21–56.

Izumiya S, Takeuchi N (2004). New special curves and developable surfaces. *Turkish Journal of Mathematics* 28: 153–164.

Kohn AJ, Riggs AC (1975). Morphometry of the *Conus* shell. *Syst Zool* 24: 346–359.

Larsson J, Westram AM, Bengmark S, Lundh T, Butlin RK, Butlin RK (2020). A developmentally descriptive method for quantifying shape in gastropod shells. *J R Soc Interface* 17. http://dx.doi.org/10.1098/rsif.2019.0721.

Liew TS, Kok ACM, Schilthuizen M, Urdy S (2014). On growth and form of irregular coiled-shell of a terrestrial snail: *Plectostoma concinnum* (Fulton, 1901) (Mollusca: Caenogastropoda: Diplommatinidae). *PeerJ* 2: e383. https://doi.org/10.7717/peerj.383.

Liew TS, Schilthuizen M (2016). A method for quantifying, visualising, and analysing gastropod shell form. *PLOS ONE* 11: 1–24. https://doi.org/10.1371/journal.pone.0157069.

Løvtrup S, Løvtrup M (1988). The morphogenesis of molluscan shells: a mathematical account using biological parameters. *J Morphol* 197: 53–62.

Løvtrup S, von Sydow B (1974). D'arcy Thompson's theorem and the shape of the molluscan shell. *Bull Math Biol* 36: 567–575.

McGhee GR (1978). Analysis of the shell torsion phenomenon in the Bivalvia. *Lethaia* 11: 315–329. https://doi.org/10.1111/j.1502-3931.1978.tb01889.x.

McGhee GR (1999). *Theoretical Morphology : The Concept and Its Applications*. Perspectives in

Earth History and Paleobiology. Columbia University Press, New York.

Monnet C, Zollikofer C, Bucher H, Goudemand N (2009). Three-dimensional morphometric ontogeny of mollusc shells by micro-computed tomography and geometric analysis. *Palaeontol Electron* 12: 1–13. https://doi.org/10.5167/uzh-23587.

Moseley H (1838). On the geometrical forms of turbinated and discoid shells. *Philosophical Transactions of the Royal Society of London* 1838: 351–370.

Moseley H (1842). On conchyliometry. *Lond Edinb Dubl Phil Mag* 21: 300–305.

Moulton D, Goriely A, Chirat R (2012). Mechanical growth and morphogenesis of seashells. *J Theor Biol* 311: 69–79. https://doi.org/10.1016/j.jtbi.2012.07.009.

Moulton DE, Goriely A (2012). Surface growth kinematics via local curve evolution. *J of Math Biol* 68: 81–108.

Naumann CF (1845). Über die wahre Spirale der Ammoniten. *Annalen der Physik* 140: 538–543. https://doi.org/10.1002/andp.18451400406.

Newkirk GF, Doyle RW (1975). Genetic analysis of shell-shape variation in *Littorina saxatilis* on an environmental cline. *Mar Biol* 30: 227–237. 10.1007/BF00390745.

Noshita K (2014). Quantification and geometric analysis of coiling patterns in gastropod shells based on 3d and 2d image data. *J Theor Biol* 363: 93–104.

Noshita K, Asami T, Ubukata T (2012). Functional constraints on coiling geometry and aperture inclination in gastropods. *Paleobiology* 38: 322–334. 10.1666/10060.1.

Noshita K, Shimizu K, Sasaki T (2016). Geometric analysis and estimation of the growth rate gradient on gastropod shells. *J Theor Biol* 389: 11–19. https://api.semanticscholar.org/CorpusID:39448122.

Nutbourne AW, Martin RR (1988). *Differential geometry applied to curve and surface design: Foundations*. Ellis Horwood, Chichester, England.

Okabe T, Yoshimura J (2017). Optimal designs of mollusk shells from bivalves to snails. *Scientific Reports* 7: 42445. https://doi.org/10.1038/srep42445.

Okamoto T (1988). Analysis of heteromorph ammonoids by differential geometry.

Paleobiology 31: 35–52.

Okamoto T (1996). Theoretical modeling of ammonoid morphology. In *Ammonoid Paleobiology* (edited by Landman NH, Tanabe K, Davis RA), pp. 225–251. Springer US, Boston, MA. https://doi.org/10.1007/978-1-4757-9153-2_8.

Páll-Gergely B, Sipos AÁ, Harzhauser M, Örstan A, Winkler V, Neubauer TA (2024). Many roads to success: alternative routes to building an economic shell in land snails. *Evolution* 78: 778–786. https://doi.org/10.1093/evolut/qpae018.

Raup DM (1961). The geometry of coiling in gastropods. *Proc Natl Acad Sci USA* 47: 602–609. https://doi.org/10.1073/pnas.47.4.602.

Raup DM (1966). Geometric analysis of shell coiling: general problems. *J Paleontol* 40: 1178–1190.

Raup DM (1967). Geometric analysis of shell coiling: coiling in ammonoids. *J Paleontol* 41: 43–65.

Raup DM, Graus RR (1972). General equations for volume and surface area of a logarithmically coiled shell. *Mathematical Geology* 4: 307–316.

Raup DM, Michelson A (1965). Theoretical morphology of the coiled shell. *Science* 147: 1294–1295.

Rice SH (1998). The bio-geometry of mollusc shells. *Paleobiology* 24: 133–149.

Savazzi E (1990). Biological aspects of theoretical shell morphology. *Lethaia* 23: 195–212.

Savazzi E (1996). Adaptaions of vermetid and siliquarid gastropods. *Palaeontology* 39: 157–177.

Schindel DE (1990). Unoccupied morphospace and the coiled geometry of gastropods: architectural constraint or geometric covariation? In *Causes of Evolution: a paleontological perspective* (edited by Ross R, Allmon W), pp. 270–304. University of Chicago Press, Chicago.

Scofield PD (1995). Curves of constant precession. *The American Mathematical Monthly* 102: 531–537. https://doi.org/10.1080/00029890.1995.12004613.

Stone JR (1995). CerioShell: a computer program designed to simulate variation in shell form. *Paleobiology* 21: 509–519.

Swan ARH (2015). Heterochrony in helicoid spiral cones: a computer model for demonstrating heterochronic evolution. *Palaeontol Electron* 18: 1–11. 10.26879/510.

Thompson DW ([1942] 1992). *On Growth and Form: The Complete Revised Edition*. Dover, New York.

Tursch B (1997). Spiral growth: The 'Museum of all shells' revisited. *J Molluscan Stud* 63: 547–554. https://doi.org/10.1093/mollus/63.4.547.

Urdy S, Goudemand N, Bucher H, Chirat R (2010). Allometries and the morphogenesis of the molluscan shell: a quantitative and theoretical model. *J Exp Zool* 314B: 280–302. 10.1002/jez.b.21337.

Uzunoğlu B, İsmail Gök, Yaylı Y (2016). A new approach on curves of constant precession. *Applied Mathematics and Computation* 275: 317–323. https://doi.org/10.1016/j.amc.2015.11.083.

van Osselaer C, Grosjean P (2000). Suture and location of the coiling axis in gastropod shells. *Paleobiology* 26: 238–257. https://doi.org/10.1666/0094-8373(2000)026<0238:SALOTC>2.0.CO;2.

Vermeij GJ (2002). Characters in context: molluscan shells and the forces that mold them. *Paleobiology* 28: 41––54.

Vinarski MV (2014). The birth of malacology. when and how? *Zoosystematics and Evolution* 90: 1–5.

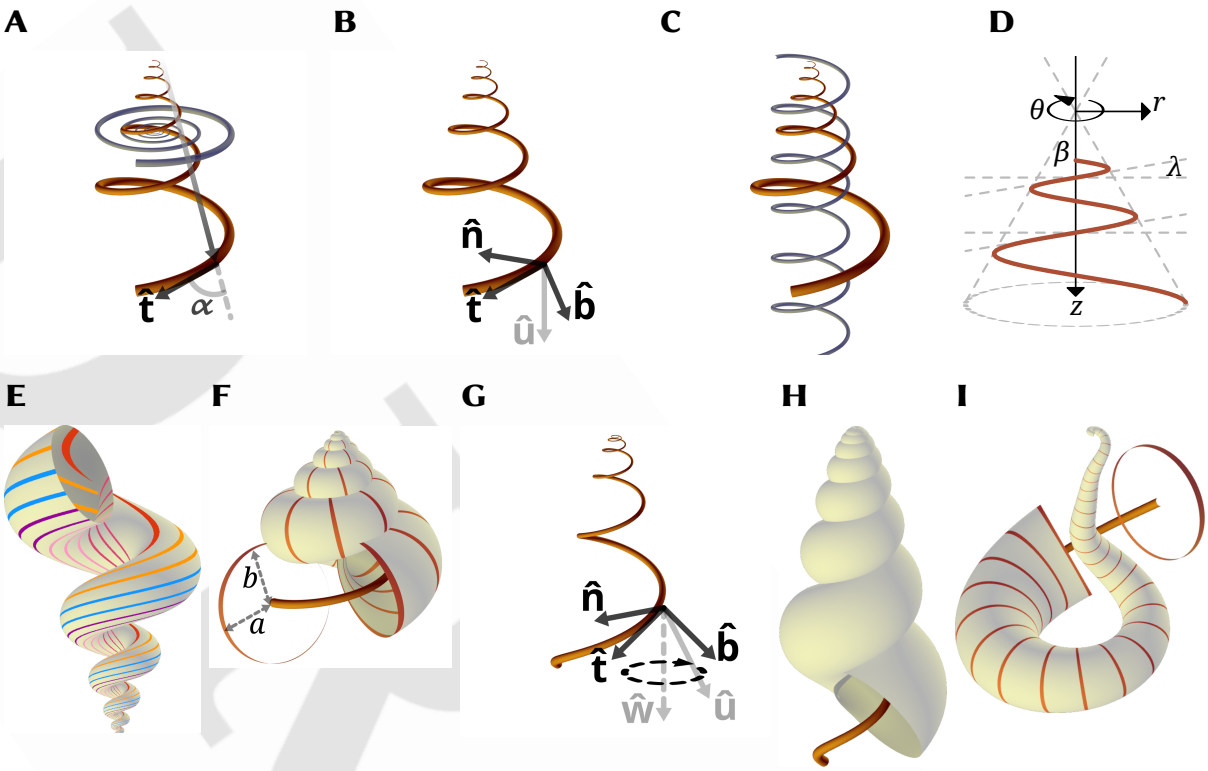

Figure 1 : Theoretical morphology in a snailshell. (***A,B,C***) Three parameterizations of conical logspirals; respectively conispiral, differential geometric, and conihelical. (***A***) Constant spiral angle, α, between instantaneous tangent vector, $\hat{\mathbf{t}}$, and radius-vector from pole (apex) defines the conispiral parameterization. The conispiral is as if a corresponding logarithmic base planispiral (in blue), with same expansion rate, γ, has been stretched out of its plane, to form a three-dimensional space curve. (***B***) The differential geometric parameterization follows the evolution of the Frenet moving frame, defined by tangent $\hat{\mathbf{t}}$, principal normal, $\hat{\mathbf{n}}$, and binormal $\hat{\mathbf{b}} = \hat{\mathbf{t}} \times \hat{\mathbf{n}}$. The frame's rotation is defined by the Darboux vector $\mathbf{u} = u\hat{\mathbf{u}} = \tau\hat{\mathbf{t}} + \kappa\hat{\mathbf{b}} = u \sin\lambda\hat{\mathbf{t}} + u\cos\lambda\hat{\mathbf{b}}$; κ is curvature, and τ torsion (SI). (***C***) In the conihelical parameterization, a conical logspiral is viewed as a helix with expanding radius – a conical helix. For comparison, a circular helix with same slope (i.e., lead angle) is also illustrated. (***D***) Conical helix in side view. Api cal semiangle, β, lead angle, λ, and the cylindrical coordinate system illustrated. The z-direction coincides with the coiling axis. (***E***) Multispiral approach to shell modeling, where shell surface is defined by many spiral paths, differing in lead angle. For illustration purposes, an exaggerated open-coiled shell is shown, where slopes of inner spirals are clearly steeper. Nevertheless, all spirals share the same expansion rate, γ. (***F***) Generating curve approach to shell modeling. Shell surface defined by a closed figure (here a circle) that sweeps along a conihelical centerline. Also illustrated are the size measures, a and b (not to be confused with the binormal vector, $\hat{\mathbf{b}}$), roughly corresponding to aperture size perpendicular and parallel, respectively, to the coiling axis. (***G***) In allometric shells, where centerline's lead angle varies, the Darboux vector is no longer fixed, but precesses around an axis $\mathbf{w} = w\hat{\mathbf{w}}$ that contains a λ' component (SI). (***H,I***) Allometric and irregularly coiled shells with logarithmic slant helix centerline. Lead angles are initially 0 (i.e., planispiral coiling), but subsequently grow at different rates. Parameters values to simulate all shell images in this figure in the `WebGL` application are provided in SI.

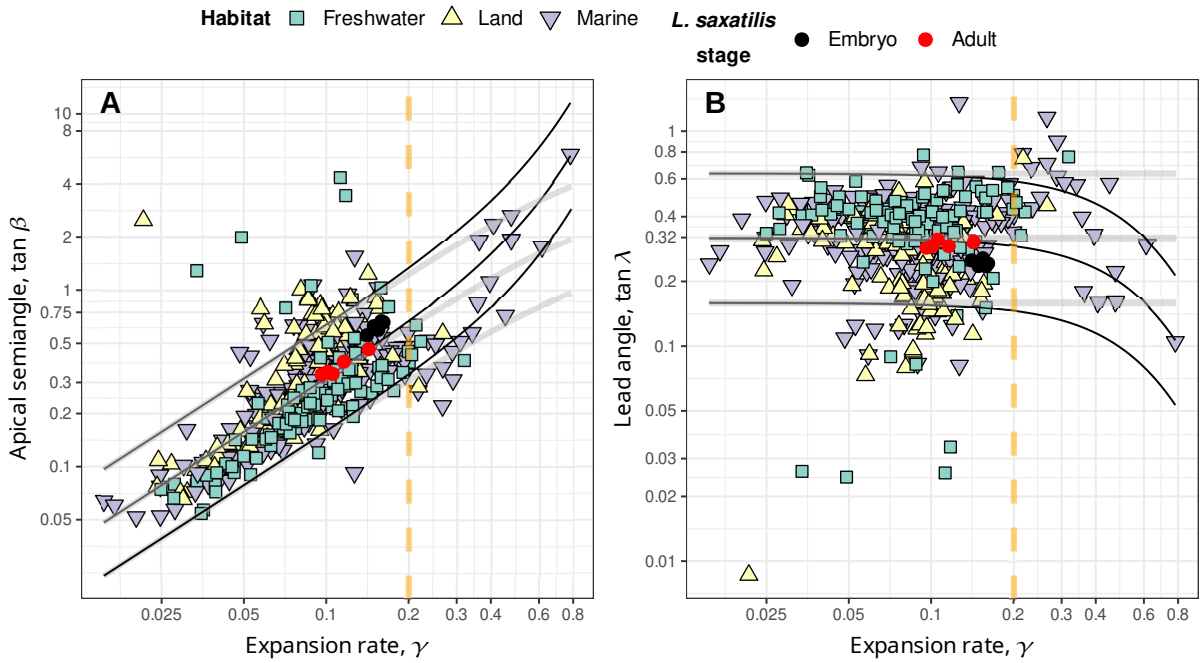

Figure 2 : Apical semiangle, as $\tan\beta$ (panel A), and lead angle, as $\tan\lambda$ (panel B), against expansion rate, $\gamma = \ln W/2\pi$, from the data in Noshita *et al.* (2012) and Araki & Noshita (2023) on coiling parameters of over 400 species freshwater, marine, and terrestrial gastropods, and the data of Newkirk & Doyle (1975) on embryos and adults of *Littorina saxatilis* from five different populations in Nova Scotia. In both panels, a vertical dashed line for $\gamma = 0.2$ marks roughly the domain of validity for small-γ approximations (SI), where nevertheless most data lies. Illustrated curves, however, were drawn using full (exact, non-approximate) expressions (SI). (***A***) When apical semiangle is plotted against expansion rate, a clear linear trend is visible. Solid black lines indicate boundaries for whorl-overlap, $\tan\beta > (1/\rho)\sinh(\pi\gamma)$, for $\rho = 0.5,\ 1,\ 2$ (upper to lower; where ρ is defined as $\rho = b/a$, ratio of the aperture sizes; $\rho = 1$ means a circular aperture) that separates tightly-coiled (above boundary line) and open-coiled shells (below boundary line). In the range $\gamma < 0.2$, such boundary curves for tight-coiling, however, are practically indistinguishable from relationships that fixed lead angles in Eq.[2] prescribe ($\tan\beta = \left(\gamma/\sqrt{1+\gamma^2}\right)\cot\lambda$; gray lines), given $\tan\lambda = \rho/\pi$ (SI; $D = 0$ for illustrated curves; i.e., apertures touching the coiling axis). Raw values for apical angles were transformed to correspond to centerlines by doubling reported values of T. (***B***) Estimates of lead angle, $\tan\lambda$, obtained from eqn:conihelical. Compared to panel A, there is clearly less in lead angle, than in apical angle, and the linear trend disappears; suggesting independent variation in expansion rate, γ, and lead angle, λ. Black and gray solid curves correspond to those those in panel A, but in reverse order ($\rho = 2,\ 1,\ 0.5$, upper to lower respectively).

Supplementary information for “Lead and slant on the geometry of coiling in gastropods”

Ido Filin *

* Corresponding author. E-mail: ido@filin.fi

Contents

S1 A note on terminology and notation 2

S2 Expressions for logarithmic conispirals 3

S3 Whorl-overlap condition for non-circular and displaced generating curves 4

S4 Approximation errors 6

S5 Differential geometric parameterization 6

S6 Logarithmic slant helix 9

S7 Web application 10

S8 Supplementary references 10

S1 A note on terminology and notation

Thompson ([1942] 1992) defined three angles, related to the modeling of equiangular (i.e., logarithmic) spiral shells. The spiral angle, α, is the angle between the radius-vector from the pole (or apex of the conical envelope) and the tangent to the spiral. His β denotes the apical semiangle, as in this study. His γ refers to the "angle of retardation", relevant when considering the inner and outer margins of planispiral shells. Given that the angle of retardation has been rarely utilized since, I reclaim the symbol γ for denoting the exponential expansion rate in this study.

Generalized or general helices (Nutbourne & Martin 1988) are defined by the constant slope, relative to a fixed direction. Hence the alternative term, curve of constant slope (Scofield 1995). Somewhat confusingly they are also often called 'cylindrical helices' (O'Neill 2006), referring to a generalized cylinder. But I avoid this term here.

While 'pitch' is used often with circular helices to refer to the slope of the helix (e.g., Chouaieb *et al.* 2006), strictly speaking, pitch is the distance between adjacent threads or strands. Lead, on the other hand, is the axial progression per one full revolution of the helical structure, which is the quantity of interest in this study. Lead and pitch are the same for single-thread helices, but not for double or triple helices, such as in double- and multi-start screws and various helical structures in biology.

The slope of the helix, $\tan\lambda$, can be measured by the lead angle, as in this study, by the 'helix slope' itself (e.g., De Renzi & Mayoral 2024; also 'rise', Hauser *et al.* 2017), or by the 'helix angle', relative to the fixed axis (the complementary angle to the lead angle; Nutbourne & Martin 1988). The latter was referred to as 'inclination angle' by Moseley (1842), in his work on conchyliometry. However, more recently, inclination angle is used to describe the orientation of the aperture itself relative to the coiling axis (Schindel 1990; Vermeij 1993; Noshita *et al.* 2012), so I avoid this term here.

Finally, the quantity $u = \sqrt{\kappa^2 + \tau^2}$, which is the norm of the Darboux vector, where κ is curvature and τ is torsion, does not have a standard name. Nutbourne & Martin (1988) refer

to it as 'compound curvature', and Güzelkardeşler & Şahiner (2024) call it 'first alternative curvatrue'. Other appropriate terms may be 'winding' or 'twist', in reference to circular helices (Chouaieb *et al.* 2006; Goriely 2017). But those usually involve additional meaning in terms of mechanical properties. It is also sometimes called angular rate, speed, or velocity, though time is only implicit here, and u measures rotation angle per unit arclength, not time. In this study, I refer to the Darboux vector and its norm, as well as to $\mathbf{w}$ and w, simply as vectors and rates of coiling, as in the end, they describe direction and rate of rotation. While the greek letter ω is often used to denote the Darboux vector and $\sqrt{\kappa^2+\tau^2}$ (Nutbourne & Martin 1988), I avoid this notation, so not to confuse with true angular velocity in mechanics.

S2 Expressions for logarithmic conispirals

Eq.[1] of the main text, $\cot\alpha \sin\beta = \gamma$, has been derived and used enough times, so not to require any explanation (Moseley 1842; Thompson [1942] 1992; Raup & Graus 1972; Løvtrup & von Sydow 1974; Ekaratne & Crisp 1983; Illert 1983). From geometry of cones, it is easy to see that

$$\sin\lambda = \cos\alpha\cos\beta \qquad [S1]$$

(Moseley 1842; up to differences in notation and definition of lead angle), the expression for spiral height dilation, q_z. These two equations can be combined to produce

$$\tan\lambda\tan\beta = \frac{\gamma}{\sqrt{1+\gamma^2}}. \qquad [S2]$$

Values of γ for gastropods are typically below 0.2 (Thompson [1942] 1992; Cameron 1981; Fig. 3), corresponding to relatively slower expansion and shells that exhibit several complete whorls. For small values of γ, Eq.[S2] is approximated by Eq.[2] of the main text.

Finally, the expression for a conispiral shell's height-to-arclength ratio, derived by Ekaratne & Crisp (1983), can be written as $(z+b)/s$ in this study, which translates to $q_z + q_b = \sin\lambda + q_b$. Alternatively, using the steps of their derivation and following the suture spiral on the outer surface of the shell, rather than the centerline spiral, $(z/W + 2b)/s = (1/W)\sin\lambda + (2\rho a/s) = (1/W)\sin\lambda + \rho r/s = \sin\lambda(1/W + \rho\tan\beta)$ (where s, r, λ and β all refer now to the suture spiral, W is the whorl expansion rate [Eq.[S3] below], and using the

relations $\rho = b/a$, $r = 2a$, and $r = z\tan\beta = s\sin\lambda\tan\beta$). In any case, all these ratios are constants for self-similar logarithmic conispiral shells.

S3 Whorl-overlap condition for non-circular and displaced generating curves

Mathematical and computational shell modeling got a boost with the work of David Raup in the 1960s (Raup 1961; Raup & Michelson 1965; Raup 1966) that also kick-started theoretical morphology. Raup's model for gastropod shell coiling (Raup 1961, 1966; Raup & Michelson 1965) contains four parameters that are designed to be estimated from sagittal cross-sections of shells. His whorl expansion rate, W, is related to γ through

$$W = e^{2\pi\gamma}. \qquad [S3]$$

His translation rate, T, is related to β by

$$T = \cot\beta. \qquad [S4]$$

The *displacement* parameter, D, measures relative distance of the aperture from the coiling axis, and is given by

$$D = \frac{r-a}{r+a}, \qquad [S5]$$

where a is aperture size in the r-direction (i.e., half the aperture's width in the r-direction). The umbilicus (or columellar) radius, ξ, i.e., distance of innermost aperture margin to the coiling axis, and the aperture size, a, are then given by

$$\begin{aligned} a &= \left(\tfrac{1-D}{1+D}\right) r, \\ \xi &= r - a = \left(\tfrac{2D}{1+D}\right) r. \end{aligned} \qquad [S6]$$

Raup's fourth parameter, S, broadly defines the shape of the generating curve, and is never really defined in Raup's formulation. In principle, it may be vector- or function-valued, e.g., $S = S(\varphi)$ (φ being some parameterization of the generating curve). It is, however, very often taken to be some ratio of major and minor axes of an ellipse — a natural extension of the circular generating curve (Raup 1966; Kohn & Riggs 1975; Newkirk & Doyle 1975; McNair *et al.* 1981; Ekaratne & Crisp 1983; Kemp & Bertness 1984; Ackerly 1992; Stone 1995; McGhee

1999; Clarke *et al.* 1999; Urdy *et al.* 2010; Larsson *et al.* 2020). Here, I follow Ekaratne & Crisp (1983) and define aperture size a, perpendicular to the coiling axis, and aperture size b, parallel to the axis, as illustrated in Fig. 1*F* of main text.

The centers of two consecutive whorls (separated by $\acute{}\theta = 2\pi$) are at distances r and rW from the coiling axis. Their distances to the apex are $r\sqrt{1+T^2}$ and $rW\sqrt{1+T^2}$, respectively. Aperture sizes along the conical envelope of the centerline spiral, i.e., at angle β to the coiling axis, are given by the radii of the elliptic generating curves at that angle $\frac{\rho a}{\sqrt{\rho^2\sin^2\beta+\cos^2\beta}}$ and $\frac{\rho aW}{\sqrt{\rho^2\sin^2\beta+\cos^2\beta}}$ respectively, where $\rho = b/a$. The whorl overlap condition is therefore,

$$r(W-1)\sqrt{1+T^2} < \frac{a\rho(W+1)\sqrt{1+T^2}}{\sqrt{\rho^2+T^2}}. \qquad [S7]$$

(recall that $T = \cot\beta$, and so $\sin^2\beta = \frac{1}{1+T^2}$ and $\cos^2\beta = \frac{T^2}{1+T^2}$). Substituting the expression for a from Eq.[S6], and further trivial manipulations give

$$T^2 < \rho^2\left(\frac{\left(\frac{1-D}{1+D}\right)^2(W+1)^2-(W-1)^2}{(W-1)^2}\right), \qquad [S8]$$

or

$$T^2 < \rho^2\frac{4W+4D^2W-4DW^2-4D}{(1+D)^2(W-1)^2}. \qquad [S9]$$

For a circular aperture ($\rho = 1$) touching the coiling axis ($D = 0$), I obtain Raup's (1966) expression for the "univalve-bivalve" boundary, $T = \frac{2\sqrt{W}}{W-1}$, on the W-T face of his morphospace cube. Substituting $T = 0$ in Eq.[S7] gives the "univalve-bivalve" boundary on the W-D face, $D < 1/W$, which is Raup's (1966) whorl-overlap condition for planispiral shells.

In terms of γ and β, Eq.[S8] can be rewritten as

$$\cot^2\beta < \rho^2\left(\left(\frac{1-D}{1+D}\right)^2\coth^2(\pi\gamma)-1\right) = \rho^2\left(\left(\frac{1-D}{1+D}\right)^2\frac{1}{\sinh^2(\pi\gamma)}-\frac{4D}{(1+D)^2}\right) \qquad [S10]$$

or

$$\tan\beta > \frac{1+D}{\rho}\frac{\sinh(\pi\gamma)}{\sqrt{(1-D)^2-4D\sinh^2(\pi\gamma)}}. \qquad [S11]$$

For circular apertures ($a = b$; $\rho = 1$) and $D = 0$, this equation gives the expression of Raup's whorl-overlap boundary in terms of γ and β of this study, $\tan\beta = \sinh(\pi\gamma)$.

From Eq.[S10] one can get the condition for whorl-overlap in terms of $\sin\beta$,

$$\sin^2\beta > \frac{1}{\rho^2\left(\frac{1-D}{1+D}\right)^2\coth^2(\pi\gamma)+(1-\rho^2)}. \quad [S12]$$

For $D=0$ this simplifies to

$$\sin^2\beta > \frac{\sinh^2(\pi\gamma)}{\sinh^2(\pi\gamma)+\rho^2}. \quad [S13]$$

For $D=0$ and $\rho=1$, the condition further reduces to $\sin\beta > \tanh\pi\gamma$, the expression arrived at by (Clarke *et al.* 1999) (after correcting their typo and accounting for difference in definition of apical semiangle).

Combining Eq.[S11] and Eq.[S2], I get the whorl-overlap boundary in terms of lead angle,

$$\tan\lambda < \frac{\rho}{1+D}\frac{\gamma\sqrt{(1-D)^2-4D\sinh^2(\pi\gamma)}}{\sqrt{1+\gamma^2}\sinh(\pi\gamma)}. \quad [S14]$$

Applying the small-γ approximation, the whorl overlap condition for lead angle becomes

$$\tan\lambda < \left(\frac{1-D}{1+D}\right)\frac{\rho}{\pi}+\mathcal{O}(\gamma^2), \quad [S15]$$

providing the corresponding fixed value of lead angle that matches the whorl overlap condition for particular aperture shape, ρ, and aperture displacement, D.

S4 Approximation errors

For the range of γ-values exhibited by most gastropods, $\gamma \leq 0.2$ (Thompson [1942] 1992; Cameron 1981), the error between the full and approximate versions of Eq.[S2] (Eq.[2] in the main text) is no more than 2%. This is derived from the ratio of the right-hand-sides of Eq.[2] and Eq.[S2], $\sqrt{1+\gamma^2}$, which clearly increases with γ, and is 1 for $\gamma=0$ and 1.0198 for $\gamma=0.2$.

S5 Differential geometric parameterization

The typical approach in differential geometry is to follow the Frenet frame, attached to a space curve; though other local (moving) frames are possible (Moulton & Goriely 2012; Moulton *et al.* 2012; Uzunoğlu *et al.* 2016; Goriely 2017; Güzelkardeşler & Şahiner 2024 ; see below). The Frenet frame is composed of the tangent, principal normal, and binormal unit vectors of the space curve, $\hat{\mathbf{t}}$, $\hat{\mathbf{n}}$, and $\hat{\mathbf{b}}$, respectively, parameterized by arclength, s, along the

curve. The frame changes along the curve according to the Frenet-Serret differential equations,

$$\begin{aligned}\hat{\mathbf{t}}' &= \frac{\mathrm{d}\hat{\mathbf{t}}}{\mathrm{d}s} = \mathbf{u}\times\hat{\mathbf{t}} = \kappa\hat{\mathbf{n}}\\ \hat{\mathbf{n}}' &= \mathbf{u}\times\hat{\mathbf{n}} = \tau\hat{\mathbf{b}} - \kappa\hat{\mathbf{t}}\\ \hat{\mathbf{b}}' &= \mathbf{u}\times\hat{\mathbf{b}} = -\tau\hat{\mathbf{n}},\end{aligned} \qquad [S16]$$

where $\times$ is vector cross-product in 3D Euclidean space, $\mathbf{u}$ is the Darboux vector,

$$\mathbf{u} = u\hat{\mathbf{u}} = \tau\hat{\mathbf{t}} + \kappa\hat{\mathbf{b}}, \qquad [S17]$$

u is the vector's magnitude (i.e., local coiling; or the compound curvature of Nutbourne & Martin 1988; see §S1), $\kappa = u\cos\lambda$ is curvature, and $\tau = u\sin\lambda$ is torsion. The Darboux vector, thus, describes the instantaneous rotation of the Frenet moving-frame, with respect to arclength (rather than time). For generalized helices ($\tau/\kappa = \tan\lambda = \text{const}$), including conical helices, the direction of the Darboux vector is fixed, $\hat{\mathbf{u}}' = 0$, though coiling rate, u, itself can change (e.g., for conical helices $u \propto 1/s$). In other words, for generalized helices $\mathbf{u}' = u'\hat{\mathbf{u}}$, and the direction $\hat{\mathbf{u}}$ determines the fixed coiling axis of the helix.

If lead angle changes with arclength, the space curve is no longer a generalized helix, and the direction of $\mathbf{u}$ changes along the curve, $\hat{\mathbf{u}}' \neq 0$ and $\mathbf{u}' = u'\hat{\mathbf{u}} + u\hat{\mathbf{u}}'$. Because $\hat{\mathbf{u}}$ is a unit vector, its derivative can be written as a cross-product with some instantaneous rotation vector, $\mathbf{w}$, such that $\hat{\mathbf{u}}' = \mathbf{w}\times\hat{\mathbf{u}}$. For generalized helices $\mathbf{w} \equiv \mathbf{u}$, and so $\hat{\mathbf{u}}' = \mathbf{u}\times\hat{\mathbf{u}} = u\hat{\mathbf{u}}\times\hat{\mathbf{u}} \equiv 0$. In the general case, we write $\mathbf{w} = w_1\hat{\mathbf{t}} + w_2\hat{\mathbf{n}} + w_3\hat{\mathbf{b}}$, and attempt to find the w_i from Eqs.[S16] and [S17].

First, note that from Eq.[S17] $\hat{\mathbf{u}} = \hat{\mathbf{t}}\sin\lambda + \hat{\mathbf{b}}\cos\lambda$, and therefore by applying the Frenet-Serret relations (Eq.[S16]), $\hat{\mathbf{u}}' = (\hat{\mathbf{t}}\cos\lambda - \hat{\mathbf{b}}\sin\lambda)\lambda'$. Expanding the rotation vector, $\mathbf{w}\times\hat{\mathbf{u}} = (-w_2\hat{\mathbf{b}} + w_3\hat{\mathbf{n}})\sin\lambda + (-w_1\hat{\mathbf{n}} + w_2\hat{\mathbf{t}})\cos\lambda$. Equating the two expressions per component, one obtains $w_2 = \lambda'$, and $w_3 = w_1\cot\lambda$, while w_1 still remains unknown. We can already guess, based on $\mathbf{w} = \mathbf{u}$ for generalized helices, that $w_1 = u\sin\lambda = \tau$ and $w_3 = u\cos\lambda = \kappa$. That is corroborated by noting that the Darboux vector does not have a $\hat{\mathbf{n}}$-component, i.e., $\hat{\mathbf{u}}$ and $\hat{\mathbf{n}}$ are always perpendicular to each other. Consequently, we can construct the alternative orthonormal moving-frame of Uzunoğlu *et al.* (2016) and

Güzelkardeşler & Şahiner (2024), composed of $\hat{\mathbf{u}}$, $\hat{\mathbf{n}}$, and $\hat{\mathbf{u}} \times \hat{\mathbf{n}}$. The rotation vector of this frame is $\mathbf{w}$, resulting in the relation $\hat{\mathbf{n}}' = \mathbf{w} \times \hat{\mathbf{n}} = w_1 \hat{\mathbf{b}} - w_3 \hat{\mathbf{t}}$. But from the Frenet-Serret equations (Eq.[S16]) we know that $\hat{\mathbf{n}}' = \tau \hat{\mathbf{b}} - \kappa \hat{\mathbf{t}}$, and so $w_1 = \tau$ and $w_3 = \kappa$, or in vector form,

$$\begin{aligned} \mathbf{w} &= w\hat{\mathbf{w}} = \mathbf{u} + \lambda' \hat{\mathbf{n}} = u\hat{\mathbf{u}} + \lambda' \hat{\mathbf{n}}, \\ w &= \sqrt{u^2 + (\lambda')^2}, \end{aligned} \qquad [S18]$$

the vector and rate of global coiling, respectively. Comparing again to Uzunoğlu *et al.* (2016) and Güzelkardeşler & Şahiner (2024), u is their 'first alternative curvature', and λ' their 'second alternative curvature'. Generalized helices are obtained when the second alternative curvature vanishes, $\lambda' = 0$ (Güzelkardeşler & Şahiner 2024). Substituting the identity $\tan\lambda = \kappa/\tau$ into their expression for the second alternative curvature, $\frac{\kappa^2}{\kappa^2+\tau^2}(\kappa/\tau)'$, clearly results in $\cos^2\lambda \, \mathrm{d}\tan\lambda/\mathrm{d}s$, which reduces to simply $\mathrm{d}\lambda/\mathrm{d}s \equiv \lambda'$. Namely, the second alternative curvature is simply the rate of change in lead angle.

For generalized helices ($\lambda = \text{const}$), $\mathbf{w} = \mathbf{u}$, $\hat{\mathbf{u}}' = \mathbf{w} \times \hat{\mathbf{u}} = -\lambda'(\hat{\mathbf{u}} \times \hat{\mathbf{n}}) = 0$, and there is a fixed coiling axis, coinciding with a fixed Darboux vector. However, in general, the vector $\mathbf{w}$ defines a precession of the Darboux vector (recall that $\mathbf{u}$ is the instantaneous rotation of the Frenet frame), and is itself not fixed. In some special cases, when $u = \text{const}$ and $\mathbf{w}$ fixed, one can obtain the 'modulated curves' of Nutbourne & Martin (1988), better known as 'curves of constant precession' (Scofield 1995).

A slant helix is, similarly, a class of precession curves that includes the generalized helix and the curves of constant precession as special cases. The defining feature of a slant helix is a constant angle between the principal normal of the curve, $\hat{\mathbf{n}}$, and some fixed direction in space. In generalized helices, that angle is 90°. Izumiya & Takeuchi's (2004) necessary and sufficient condition for a slant helix translates, in the notation of this study, to the proportionality relationship $\lambda' = \sigma u$. In other words, second alternative curvature is proportional to first alternative curvature, with a proportionality constant σ. The global coiling vector becomes $\mathbf{w} = w\hat{\mathbf{w}} = u(\hat{\mathbf{u}} + \sigma\hat{\mathbf{n}})$, and $\hat{\mathbf{w}}$ defines a fixed axis of rotation (or coiling), though coiling rate, $w = u\sqrt{1+\sigma^2}$, around the fixed axis generally varies. That can be verified by $\sqrt{1+\sigma^2}\hat{\mathbf{w}}' = (\hat{\mathbf{u}} + \sigma\hat{\mathbf{n}})' = \mathbf{w} \times \hat{\mathbf{u}} + \sigma\mathbf{w} \times \hat{\mathbf{n}} = (\sigma u\hat{\mathbf{n}}) \times \hat{\mathbf{u}} + \sigma(u\hat{\mathbf{u}} \times \hat{\mathbf{n}}) = 0$.

Finally, note that the lead angle, λ, is defined in the $\hat{\mathbf{t}}$-$\hat{\mathbf{b}}$ plane, the *rectifying plane* of the space curve. For generalized helices, this plane contains the coiling axis, i.e. z-axis, and lead angle therefore is the angle between $\hat{\mathbf{t}}$ and the r-θ (or x-y) plane, perpendicular to the coiling axis; or the z-component of $\hat{\mathbf{t}}$ is $\sin\lambda$. That is no longer the case for slant helices. The rectifying plane now revolves around the coiling axis at a fixed tilt angle, given by $\arctan(\sigma)$. Lead angle is still defined in the rectifying plane, and therefore the tangent vector, $\hat{\mathbf{t}}$, which is also the unit velocity vector of the space curve w.r.t to arclength, is given in Cartesian coordinates by

$$\begin{aligned}\hat{\mathbf{t}} &= (-\cos\lambda\sin\theta + c\sin\lambda\cos\theta)\,\hat{\mathbf{x}} + (\cos\lambda\cos\theta + c\sin\lambda\sin\theta)\,\hat{\mathbf{y}} + \sqrt{1-c^2}\sin\lambda\hat{\mathbf{z}},\\ c &= \frac{\sigma}{\sqrt{1+\sigma^2}} = \text{const},\end{aligned} \qquad \text{[S19]}$$

where $\lambda = \lambda(s)$ and $\theta = \theta(s)$.

S6 Logarithmic slant helix

For the logarithmic slant helix, $u = \tilde{u}/s$. Consequently, $\lambda' = \sigma\tilde{u}/s$ and $w = \tilde{w}/s$, where $\tilde{w} = \tilde{u}\sqrt{1+\sigma^2}$. Given that $\mathrm{d}\theta/\mathrm{d}s = w$, it is straightforward to get relations comparable to conical helices for revolution angle and arclength, $\theta = \tilde{w}\ln(s/s_0)$ and $s = s_0 e^{\gamma\theta}$, where $\gamma = 1/\tilde{w}$ (in this section, $\gamma \equiv \gamma_s$). Given $\lambda' = \mathrm{d}\lambda/\mathrm{d}s = \sigma u = cw = c\,\mathrm{d}\theta/\mathrm{d}s$ (c as in Eq.[S19]), lead angle increases linearly with revolution angle according to $\lambda = \lambda_0 + c\theta$. From these expressions one can obtain the position vector of the logarithmic slant helix, $x(\theta)\hat{\mathbf{x}} + y(\theta)\hat{\mathbf{y}} + z(\theta)\hat{\mathbf{z}}$, by integrating $(\mathrm{d}s/\mathrm{d}\theta)\hat{\mathbf{t}}(s)$ w.r.t to θ, given Eq.[S19] for $\hat{\mathbf{t}}(s)$,

$$z(\theta) = C_z + \sqrt{1-c^2}\,s_0 e^{\gamma\theta}\left(\frac{\gamma^2\sin(c\theta+\lambda_0) - c\gamma\cos(c\theta+\lambda_0)}{c^2+\gamma^2}\right), \qquad \text{[S20]}$$

$$\begin{aligned}x(\theta) = C_x + \frac{\gamma s_0 e^{\gamma\theta}}{c^4 + 2c^2\gamma^2 - 2c^2 + \gamma^4 + 2\gamma^2 + 1}(&-c^4\cos\lambda\cos\theta + c^3\gamma\sin\lambda\cos\theta - 2c^3\sin\lambda\sin\theta\\ &- c^2\gamma^2\cos\lambda\cos\theta - 3c^2\gamma\sin\theta\cos\lambda + c\gamma^3\sin\lambda\cos\theta + 3c\gamma\sin\lambda\cos\theta + 2c\sin\lambda\sin\theta\\ &- \gamma^3\sin\theta\cos\lambda + \gamma^2\cos\lambda\cos\theta - \gamma\sin\theta\cos\lambda + \cos\lambda\cos\theta),\end{aligned} \qquad \text{(S21)}$$

$$\begin{aligned}y(\theta) = C_y + \frac{\gamma s_0 e^{\gamma\theta}}{c^4 + 2c^2\gamma^2 - 2c^2 + \gamma^4 + 2\gamma^2 + 1}(&-c^4\sin\theta\cos\lambda + c^3\gamma\sin\lambda\sin\theta + 2c^3\sin\lambda\cos\theta\\ &- c^2\gamma^2\sin\theta\cos\lambda + 3c^2\gamma\cos\lambda\cos\theta + c\gamma^3\sin\lambda\sin\theta + 3c\gamma\sin\lambda\sin\theta\\ &- 2c\sin\lambda\cos\theta + \gamma^3\cos\lambda\cos\theta + \gamma^2\sin\theta\cos\lambda + \gamma\cos\lambda\cos\theta + \sin\theta\cos\lambda),\end{aligned} \qquad \text{(S22)}$$

where C_z, C_x, C_y are determined from initial conditions. These expressions for $x(\theta)$, $y(\theta)$ and $z(\theta)$, can be used in computer graphics to simulate shells that follow a logarithmic slant helix centerline.

S7 Web application

For this study, I have also written a `WebGL` application to help with creating images of shells, as in Fig. 1*A–C,E–I*. A snapshot of the code, coinciding with the publication of this report, is available at https://doi.org/10.5281/zenodo.19895626.

- For Fig. 1*A–C*, Shell unchecked, Centerline spiral checked, Generating curve unchecked, and either Planispiral (panel A) or Circular helix (panel C) additionally selected. Pitch angle 69°, Roll angle 200°, $\lambda_0 = 0.22$, $\tilde{w} = 11.43$ ($\gamma = 0.0875$), $\sigma = 0$.
- Parameters for Fig. 1*E* are Pitch angle 270, Roll angle 64, Shell and Multispirals checked, Generating curve unchecked. $\lambda_0 = 0.39$, $\tilde{w} = 9.38$ ($\gamma = 0.107$), $\sigma = 0$.
- For Fig. 1*F*, Pitch angle 70, Roll angle 257. Shell, Centerline spiral, and Generating curve checked. $\lambda_0 = 0.22$, $\tilde{w} = 11.43$ ($\gamma = 0.0875$), $\sigma = 0$.
- Parameters for Fig. 1*G* are Pitch angle 69, Roll angle 300, Shell deselected, Centerline spiral checked, Generating curve unchecked, $\lambda_0 = 0$, $\tilde{w} = 11.43$ ($\gamma = 0.0875$), $\sigma = 0.013$.
- Parameters for Fig. 1*H* are Pitch angle 69, Roll angle 36, Shell deselected, Centerline spiral checked, Generating curve unchecked, $\lambda_0 = 0$, $\tilde{w} = 18.99$ ($\gamma = 0.0527$), $\sigma = 0.01$.
- For Fig. 1*I*, Pitch angle 62, Roll angle 152, Shell, Centerline spiral, and Generating curve checked, $\lambda_0 = 0$, $\tilde{w} = 5.85$ ($\gamma = 0.171$), $\sigma = 0.21$.

S8 Supplementary references

Ackerly SC (1992). The structure of ontogenetic variation in the shell of *Pecten*. *Palaeontology* 35: 847–867.

Cameron RAD (1981). Functional aspects of shell geometry in some british land snails. *Biol J Linn Soc* 16: 157–167. https://doi.org/10.1111/j.1095-8312.1981.tb01648.x.

S240 Chouaieb N, Goriely A, Maddocks JH (2006). Helices. *Proc Natl Acad Sci USA* 103: 9398–9403.
S241 https://doi.org/10.1073/pnas.0508370103.
S242 Clarke RK, Grahame J, Mill PJ (1999). Variation and constraint in the shells of two sibling
S243 species of intertidal rough periwinkles (gastropoda: Littorina spp.). *J Zool* 247: 145–154.
S244 10.1111/j.1469-7998.1999.tb00978.x.
S245 De Renzi M, Mayoral E (2024). Understanding behaviour through theoretical morphology:
S246 the case of helical-shaped burrows. *J Iber Geol* 50: 549–566.
S247 https://doi.org/10.1007/s41513-024-00249-7.
S248 Ekaratne SUK, Crisp DJ (1983). A geometric analysis of growth in gastropod shells, with
S249 particular reference to turbinate forms. *Journal of Marine Biology Association UK* 63:
S250 777–797.
S251 Goriely A (2017). *The Mathematics and Mechanics of Biological Growth*. Springer.
S252 https://doi.org/10.1007/978-0-387-87710-5.
S253 Güzelkardeşler G, Şahiner B (2024). An alternative approach to find the position vector of a
S254 general helix. *Celal Bayar University Journal of Science* 20: 54–60.
S255 10.18466/cbayarfbe.1479066.
S256 Hauser K, He Y, Garcia-Diaz M, Simmerling C, Coutsias E (2017). Characterization of
S257 biomolecular helices and their complementarity using geometric analysis. *Journal of*
S258 *Chemical Information and Modeling* 57: 864–874.
S259 https://doi.org/10.1021/acs.jcim.6b00721. PMID: 28287728.
S260 Illert C (1983). The mathematics of gnomonic seashells. *Math Biosci* 63: 21–56.
S261 Izumiya S, Takeuchi N (2004). New special curves and developable surfaces. *Turkish Journal*
S262 *of Mathematics* 28: 153–164.
S263 Kemp P, Bertness MD (1984). Snail shape and growth rates: evidence for plastic shell
S264 allometry in *Littorina littorea*. *Proc Natl Acad Sci USA* 81: 811–813.
S265 https://doi.org/10.1073/pnas.81.3.811.
S266 Kohn AJ, Riggs AC (1975). Morphometry of the *Conus* shell. *Syst Zool* 24: 346–359.

Larsson J, Westram AM, Bengmark S, Lundh T, Butlin RK, Butlin RK (2020). A developmentally descriptive method for quantifying shape in gastropod shells. *J R Soc Interface* 17. http://dx.doi.org/10.1098/rsif.2019.0721.

Løvtrup S, von Sydow B (1974). D'arcy Thompson's theorem and the shape of the molluscan shell. *Bull Math Biol* 36: 567–575.

McGhee GR (1999). *Theoretical Morphology : The Concept and Its Applications*. Perspectives in Earth History and Paleobiology. Columbia University Press, New York.

McNair C, Kier W, LaCroix P, Linsley R (1981). The functional significance of aperture form in gastropods. *Lethaia* 14: 63–70.

Moseley H (1842). On conchyliometry. *Lond Edinb Dubl Phil Mag* 21: 300–305.

Moulton D, Goriely A, Chirat R (2012). Mechanical growth and morphogenesis of seashells. *J Theor Biol* 311: 69–79. https://doi.org/10.1016/j.jtbi.2012.07.009.

Moulton DE, Goriely A (2012). Surface growth kinematics via local curve evolution. *J of Math Biol* 68: 81–108.

Newkirk GF, Doyle RW (1975). Genetic analysis of shell-shape variation in *Littorina saxatilis* on an environmental cline. *Mar Biol* 30: 227–237. 10.1007/BF00390745.

Noshita K, Asami T, Ubukata T (2012). Functional constraints on coiling geometry and aperture inclination in gastropods. *Paleobiology* 38: 322–334. 10.1666/10060.1.

Nutbourne AW, Martin RR (1988). *Differential geometry applied to curve and surface design: Foundations*. Ellis Horwood, Chichester, England.

O'Neill B (2006). *Elementary Differential Geometry*. Revised 2nd edn. Academic Press.

Raup DM (1961). The geometry of coiling in gastropods. *Proc Natl Acad Sci USA* 47: 602–609. https://doi.org/10.1073/pnas.47.4.602.

Raup DM (1966). Geometric analysis of shell coiling: general problems. *J Paleontol* 40: 1178–1190.

Raup DM, Graus RR (1972). General equations for volume and surface area of a logarithmically coiled shell. *Mathematical Geology* 4: 307–316.

S294 Raup DM, Michelson A (1965). Theoretical morphology of the coiled shell. *Science* 147:
S295 1294–1295.
S296 Schindel DE (1990). Unoccupied morphospace and the coiled geometry of gastropods:
S297 architectural constraint or geometric covariation? In *Causes of Evolution: a paleontological*
S298 *perspective* (edited by Ross R, Allmon W), pp. 270–304. University of Chicago Press,
S299 Chicago.
S300 Scofield PD (1995). Curves of constant precession. *The American Mathematical Monthly* 102:
S301 531–537. https://doi.org/10.1080/00029890.1995.12004613.
S302 Stone JR (1995). CerioShell: a computer program designed to simulate variation in shell form.
S303 *Paleobiology* 21: 509–519.
S304 Thompson DW ([1942] 1992). *On Growth and Form: The Complete Revised Edition.* Dover,
S305 New York.
S306 Urdy S, Goudemand N, Bucher H, Chirat R (2010). Allometries and the morphogenesis of the
S307 molluscan shell: a quantitative and theoretical model. *J Exp Zool* 314B: 280–302.
S308 10.1002/jez.b.21337.
S309 Uzunoğlu B, İsmail Gök, Yaylı Y (2016). A new approach on curves of constant precession.
S310 *Applied Mathematics and Computation* 275: 317–323.
S311 https://doi.org/10.1016/j.amc.2015.11.083.
S312 Vermeij GJ (1993). *A Natural History of Shells.* Princeton University Press, Princeton, Oxford.